Final Draft
of the original manuscript:

Crack retardation mechanism due to overload in base material and laser welds of Al alloys

S. Daneshpour[1], J. Dyck[2], V. Ventzke[1], N. Huber[1]

[1] GKSS Research Centre, Institute of Materials Research, Geesthacht, Germany

[2] University of Waterloo, Dep. of Mechanical Engineering, Waterloo, Canada

Abstract

In order to determine retardation mechanisms due to overload and to predict the subsequent evolution of crack growth rate, investigations are conducted on crack retardation due to single tensile overload in laser weld and base material of AA6056-T6 Al alloys sheets. The effect of such overloads with different load ratios on the fatigue crack propagation behavior of the homogenous base metal and welded C(T) 100 specimens was compared in terms of crack growth rate and fracture surface features using experimental and FE analysis methods. The retardation due to overload is described in term of affected regions ahead of the crack tip. The size and shape of the crack tip plastic zone and the damage profile induced during the application of the overload in base material are predicted by FE analysis in conjunction with a porous metal plasticity model. The results show that the mechanisms of retardation in under-matched welds are substantially different from that of homogenous base material. The more significant crack retardation due to overload has been observed in the laser weld of AA6056-T6. Based on SEM observations of fracture surfaces and damage profiles predicted by the proposed FE model, the shape of the crack front formed during the application of overload can be correlated. During the overload, the crack-front extends to a new shape which can be predicted by the ductile damage model; the higher the load the more curved the resulting crack-front. These outcomes are used to determine the dominated retardation mechanisms and the significance of retardation observed in each region ahead of crack tip and finally to define the minimum crack growth rate occurred after overload.

Keywords: Overloads; Fatigue crack growth; Weld metal; Aluminium alloys; Damage.

1. Introduction

Aircraft structures operate under spectrum loading (variable amplitude cyclic loading) where load history effects occur. The occurrence of an overload (high-low load sequence) has strong effects on the crack propagation behaviour; tensile overloads lead to favourable crack retardation or even crack arrest specifically in laser welded Al sheets [1]. The reliability of fatigue life prediction methods mainly depends on their ability to account for the mechanisms of damage taking place during cyclic loading. The accurate understanding of the mechanism for the load-interaction effects and its consequence on degradation of material ahead of crack tip and its interaction with ongoing fatigue crack growth is essential for the damage tolerance design and the development of the lifetime prediction model. Conventional fatigue life calculations, e.g. using the Miner rule [2], lead to either non-conservative or an under-prediction of the real fatigue life. Improvements to life prediction can be made by adding the effect of loads interaction that is always occurring in a load spectrum, to increase the accuracy of life prediction methods.

Laser beam welding (LBW) is already being used in several aircraft structures to reduce weight and fabrication cost by replacing the conventional riveting technology [3-4]. By use of the LBW technology, it is currently practised to fabricate integral stiffened panels containing T-joints between stringer and skin sheet. This advanced LBW technology is capable of produce highly complex and competitive airframe parts for current and future metallic aircrafts [5]. In order to extend the current application area of the welded panels, it is essential to improve current level of knowledge on the damage tolerance performance of the welded Al-alloy components. Here, fatigue crack propagation (FCP) is one of the main areas of interest to improve structural performance of the aircrafts. Knowingly, damage tolerance design concepts based on FCP performance are important to describe design life and inspection intervals.

Crack retardation due to tensile overload is one particular phenomenon that makes the damage accumulation dependent on the sequence of the stress time series. A typical effect of overload on extension of fatigue life (N_D) is schematically shown in Fig. 1a. According to the Fig. 1b, delay in crack growth rate due to an overload can be divided to the two separate phases [6]: Phase 1 occurres directly after applying overload (point S in the Fig. 1b) and is due to the loading cycle dependence effect, on which growth rate decreases to reach to the minimum growth rate (point M in the Fig. 1b). Phase 2 is due to the crack growth dependence

effect. Total restoration of the crack growth rate (until point R in the Fig. 1b) may occur under one of the described paths in the Fig. 1b.

a)

b)
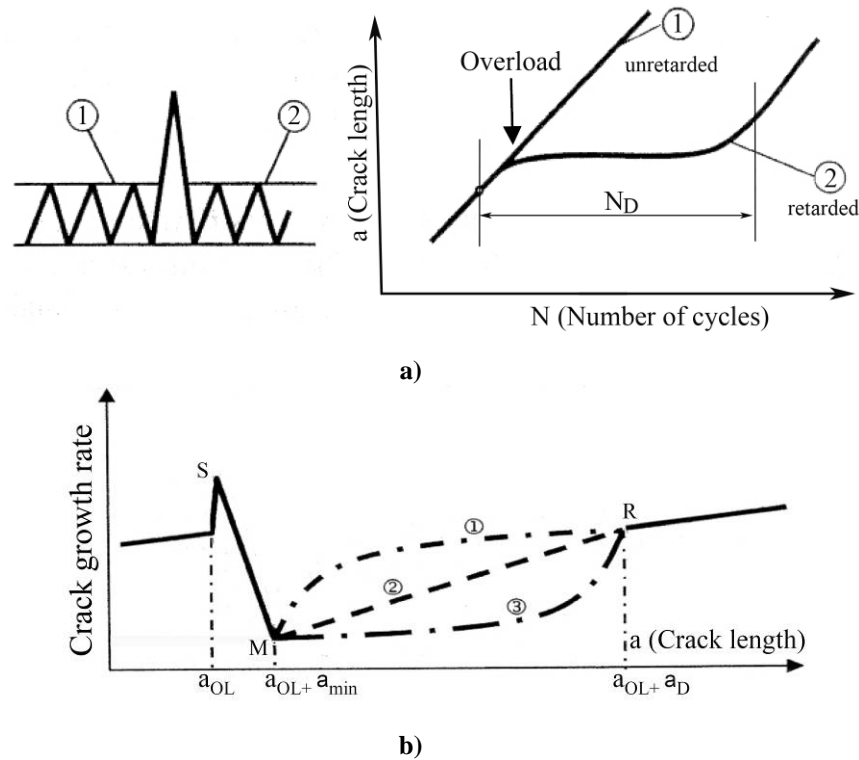
Fig. 1. a) Typical fatigue life extension (N_D) due to an overload, b) delay in crack growth rate after overload [6]

Two aspects that support the study of overload (OL) effects (or in a more general term, load interaction effects) on fatigue crack growth are summarized below:

I) Development of damage tolerance design and accurate life prediction of aircraft components under variable amplitude loads require a deep understanding of the micro-mechanism of crack retardation due to OL. The delay phenomenon of the crack growth in fatigue following an OL, although discovered and explained by numerous researchers [7-12], remains only partially understood. Due to the lack of experimental capabilities to measure stress/strain fields within the bulk material under applied load, the relationship between overload and retardation has not yet been quantitatively established.

II) Overload can be used as a way for improving the fatigue performance of welded structures where the weld metal is softer than the base material. It has been shown that the application of a single overload (SOL) during cyclic loading may cause a significant decrease in the crack growth rate or even full arrest of the crack [1].

The cause for the crack retardation due to overload can be explained by several phenomena such as crack deflection and bifurcation, crack tip blunting [13], strain hardening of the material at the crack tip [14], crack closure (induced by plasticity[15], roughness or

oxidation), and compressive residual stresses ahead of crack tip [16]. Among these mechanisms, crack closure induced by plasticity and compressive residual stresses ahead of the crack tip are widely accepted as the main retardation mechanisms due to overload and are being widely used for modeling of crack growth after an overload. Although, it is not correct to consistently attribute any one mechanism to the retardation phenomenon in general. The problem is even more complicated in the case of welded components, since the material heterogeneity and residual stresses caused by the welding process influence the crack propagation rate as well, but their effect can not be treated independently from that of an overload.

There is currently little explanation found in literature for the delayed effect of crack retardation due to an overload, particularly the deceleration part of the curve (S-M path in Fig. 1b) and the exact value and location of point M at minimum crack growth rate (a_{min}). In this study, investigations were carried out to understand the mechanisms of fatigue crack growth retardation due to an overload and to provide evidences determining value and location of the minimum crack growth rate. This aims at developing a reliable fatigue life prediction that is a central theme in the design of aerospace components and assemblies. Finite Element simulations in conjunction with experimental tools, such as scanning electron microscopy and an optical plastic strain measurement, have been used to analyze the fracture surface and to provide a better understanding of the dominant retardation mechanisms due to overload. In the following sections, the effects of an overload on crack growth rate and shape of the crack front in standard Compact-Tension specimens, C(T) 100, are discussed for laser welded/non-welded AA6056-T6 sheets.

2. Methods

2.1. Experimental details

The material used in this study was AA6056-T6 aluminum alloys sheet with thickness of 6.1 mm; the 6xxx series of aluminum alloy, with the primary alloying components of magnesium and silicon, grant a good weldability. The aluminum sheets were welded with CO_2 Laser beam welding in the butt joint configuration with a full penetration. Details of the welding parameters and the weld configuration are explained in Ref. [17].

To determine the effect of a single overload on fatigue crack retardation, standard Compact Tension specimen, C(T) 100, prepared in accordance with the standard test method for measurement of fatigue crack growth rates [18] have been used. The dimensions of the

weld and base material specimens are shown in Fig. 2. A 25 kN servo-hydraulic universal testing machine was used to perform the fatigue experiments. A travelling microscope consisting of a microscope with a 10X magnification attached to two micrometers with resolutions of 0.01 mm was used to measure incremental fatigue crack growth from both sides of the C(T) specimens. The fatigue loading applied to the specimens was comprised of axial loading in a sinusoidal wave form at room temperature in air.
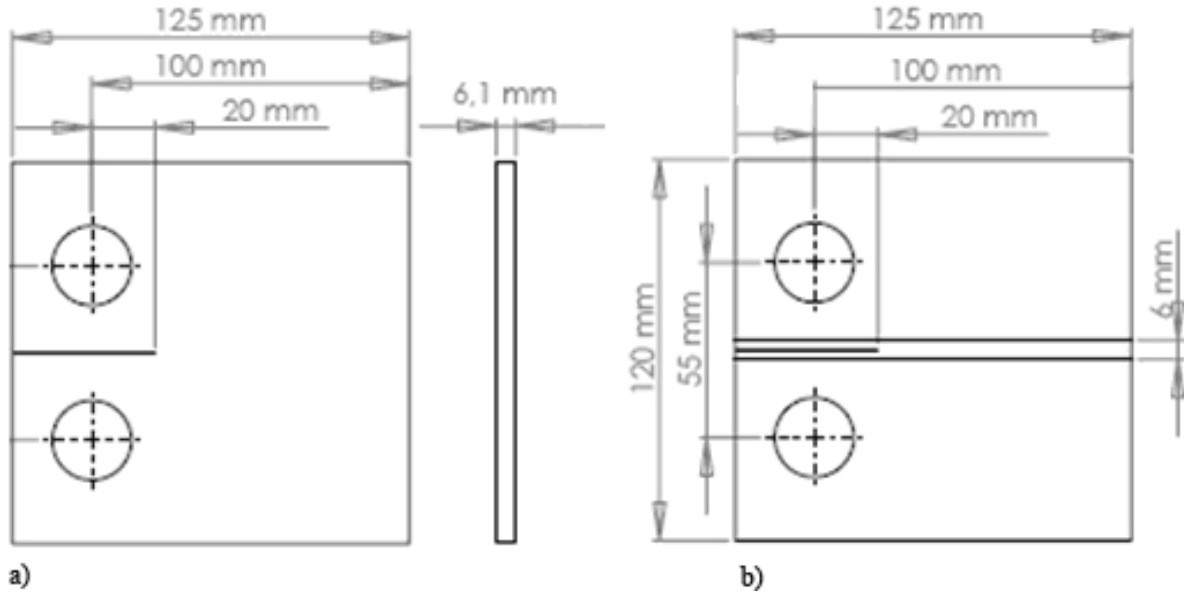

Fig. 2. Geometry of C(T) 100 specimens used in this study: a) Base material, b) Laser welded specimen

The fatigue crack growth test was conducted as follows:

- The baseline constant amplitude loading consisted of cycles at maximum load, F_{max}, of 5.1 kN and load ratio of $R = 0.1$ with a load frequency of 10 Hz; this ccorresponded to the stress intensity factor range of $\Delta K = 10\, MPa\sqrt{m}$ at initial crack length of 20 mm.
- When the crack grew to a specific length (a=30mm) the single overload was applied. Two overload ratios ($R_{OL} = F_{OL} / F_{max}$) were used: R_{OL}=2 corresponding to F_{OL}=10.2 kN and R_{OL}=2.5 corresponding to F_{OL}=12.4 kN.
- Cyclic loading with a $\Delta K = 10\, MPa\sqrt{m}$ continued at the constant amplitude loading until failure.

Fig. 3 summarizes the load sequence applied to the C(T) 100 specimens.
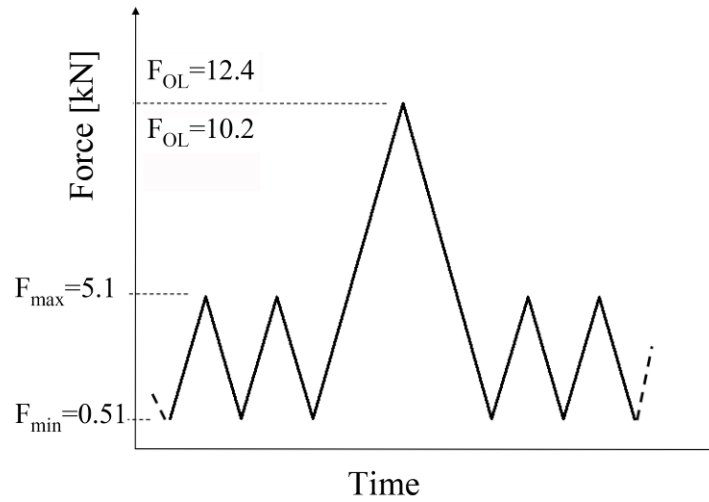
Fig. 3. Load sequence describing the overload and the constant amplitude loading applied to the C(T) 100 specimens

2.2. Finite Element model

A 3D Finite Element analysis was performed to predict the damage profile resulting from a single overload in the C(T) 100 specimen of base material. Considering the symmetries, only half of the C(T) 100 specimen was modeled. The finite element model consists of linear hexahedral elements available in ABAQUS FE software. Fig. 4 shows a zoom into the 3D finite element mesh of linear hexahedral elements. In vicinity of crack tip the finest elements are 0.05 mm in size.
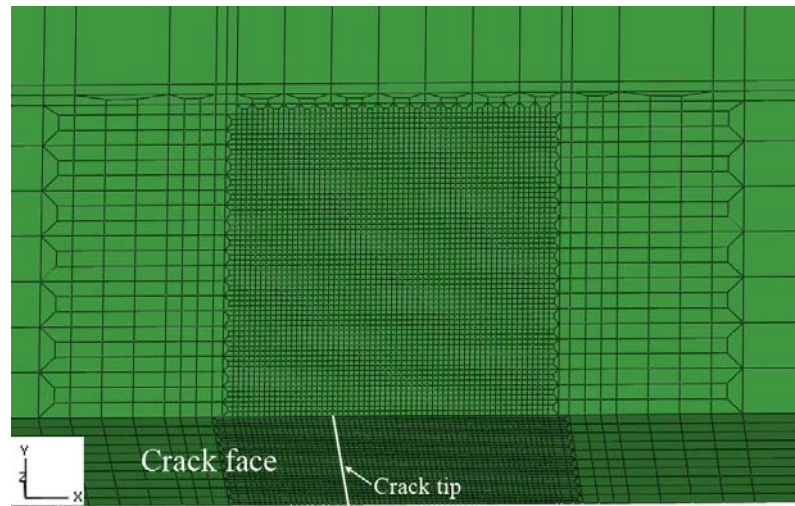

Fig. 4. Fine meshed (3D) region around the crack tip with a size of 0.05 mm

The FE analysis was conducted using a GTN model consisting of porous metal plasticity with nonlinear isotropic hardening. The porous metal plasticity model assumes an

isotropic ductile damage based on void nucleation, growth and coalescence where the yield condition is given in the form proposed by Gurson [19]

$$\left(\frac{q}{\sigma_y}\right)^2 + 2q_1 f \cosh\left(-\frac{3}{2}\frac{q_2 p}{\sigma_y}\right) - \left(1 + q_3 f^2\right) = 0, \tag{1}$$

where q is von Mises stress (deviatoric part of stress tensor that tends to distort elements), σ_y is yield stress of fully dense matrix material, p is hydrostatic pressure that tend to nucleation, growth and coalescence of voids and f represents volume fraction of the voids. The parameters q_1, q_2 and q_3 are material constants that need to be fitted to the material used in this study: AA6056-T6. In Fig. 5, the mechanical response of a C(T) specimen under uniaxial loading is compared with the proposed FE model after fitting parameters required in Eq. 1 for the GTN model. The values obtained for the q_1, q_2 and q_3 material constants are 1, 1.32 and 1 respectively. Three parameters related to the void nucleation and two parameters related to the porous failure criteria were also adjusted. Figure 5 reveals good agreement between simulation and experimental results showing capability of the proposed FE model for prediction of the global Force-CMOD response of the material used in this study. In the next step, this model can be applied to determine the local damage distribution, plastic zone and residual stress field caused by application of a single overload in the C(T) 100-specimens of base material.

a)   b)
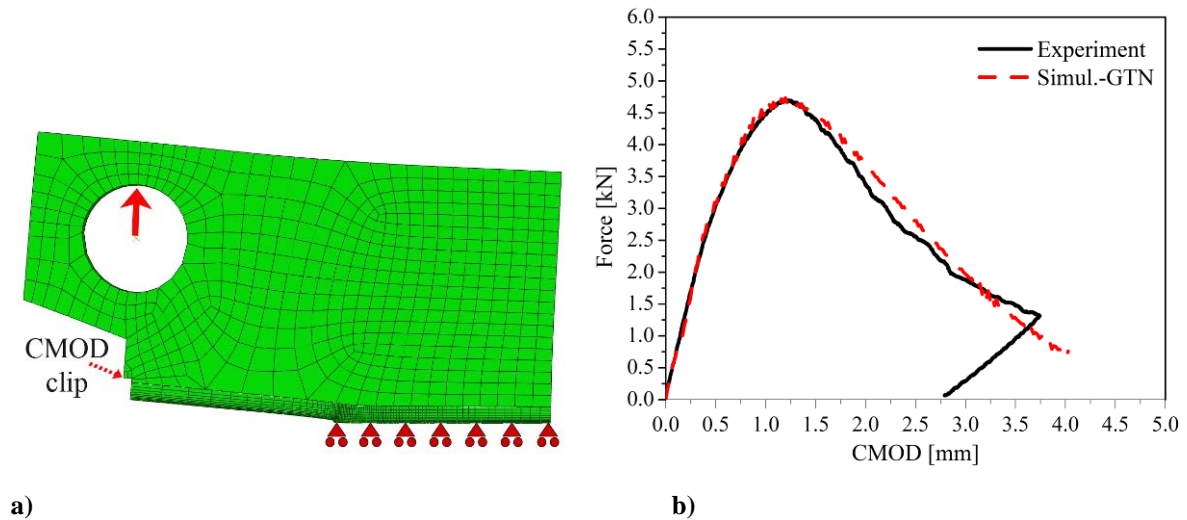
Fig. 5. a) FE model used to determine fitting parameters of the GTN model, b) Mechanical response of base material (black solid line represents average of 3 samples) in comparison with the FE simulation after fitting material parameters of the GTN model (dashed red line)

3. Results and discussions

3.1. Fatigue crack propagation

The total fatigue lives of base material and laser welded AA6056-T6 specimen subjected to the loading scenario, as explained in the Section 2.1 and shown in the Fig. 3, are summarized in Table 1. The results show that the crack retardation is more pronounced for high overload ratios. Fatigue lives of welded specimen are 4.6 times and 4.9 times higher than those of base material for overload ratios of R_{OL}=2 and R_{OL}=2.5, respectively.

Table 1. Total fatigue lives of base and weld material; $R_{OL} = F_{OL}/F_{max}$

Total fatigue life	R_{OL} =2		R_{OL} =2.5	
	Base material	Weld material	Base material	Weld material
Number of Cycles until failure	$1.24.10^5$	$5.67 \cdot 10^5$	$8.07 \cdot 10^5$	$3.95 \cdot 10^6$

Overload induced plastic strains were measured by an optical strain measurement system ARAMIS from a region in vicinity of the crack tip in both types of specimens (weld and base material). Fig. 6a shows the development of the crack tip plastic zones measured from the surfaces of the C(T) 100 specimens during various stages of the overload at load levels given in Fig. 6b.
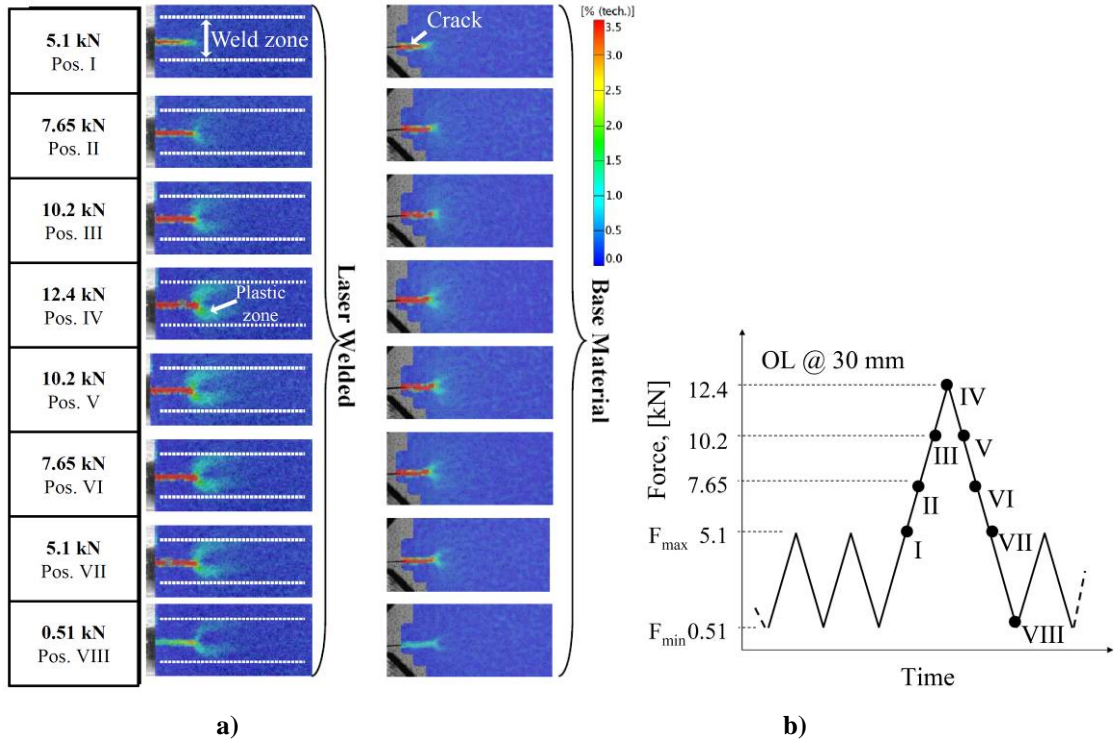
Fig. 6. a) Development of the crack tip plastic zones in laser weld and base material subjected to the single overload at load levels shown in Fig. 6 b).

According to the Fig. 6a, the size of plastic zone in the weld material is visibly larger than in base material for all load levels. It can also be seen in the shape of the plastic zone in the welded specimens that the plastic deformation ahead of the crack tip is confined to the weld zone. This phenomenon has been explained in more detail elsewhere [1]. The confined crack tip plasticity observed in laser welded Al alloys is a result of the undermatching characteristic of the laser weld due to reduced yield stress. The application of a tensile overload induces plastic deformation, which is stronger, but confined to the weld zone. As a consequence, it is elongated ahead of the crack tip resulting in significant crack retardation and longer fatigue life in the laser welded specimens as observed in the Table 1.

Since the mechanisms of the delay phenomenon under consideration are a result of a tensile overload, the effect increases with increasing overload ratio. However, a quantitative estimation of the effect or a statement on the nature of the nonlinear dependence can not be easily given. Figs. 7 and 8 reveal the crack growth rate as a function of crack length in the base material and weld material that clearly show the delay phenomenon for crack growth after applying the tensile overload.
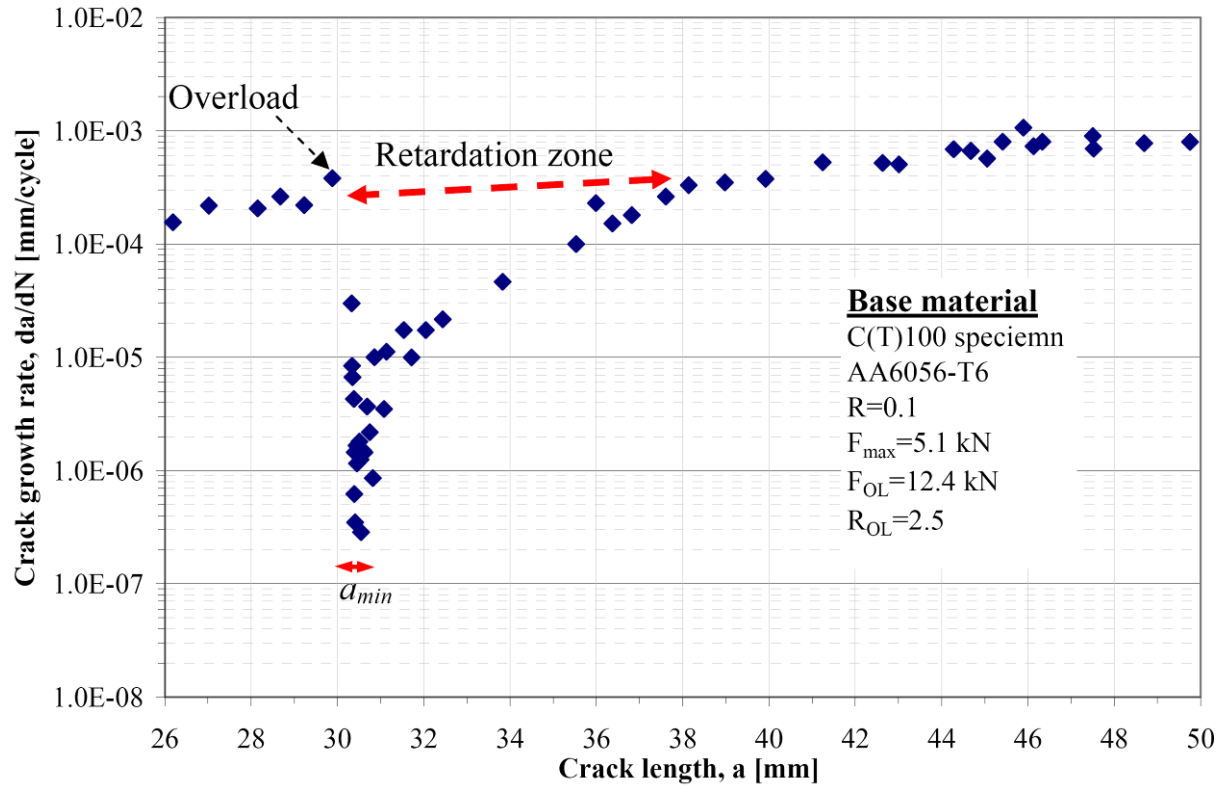

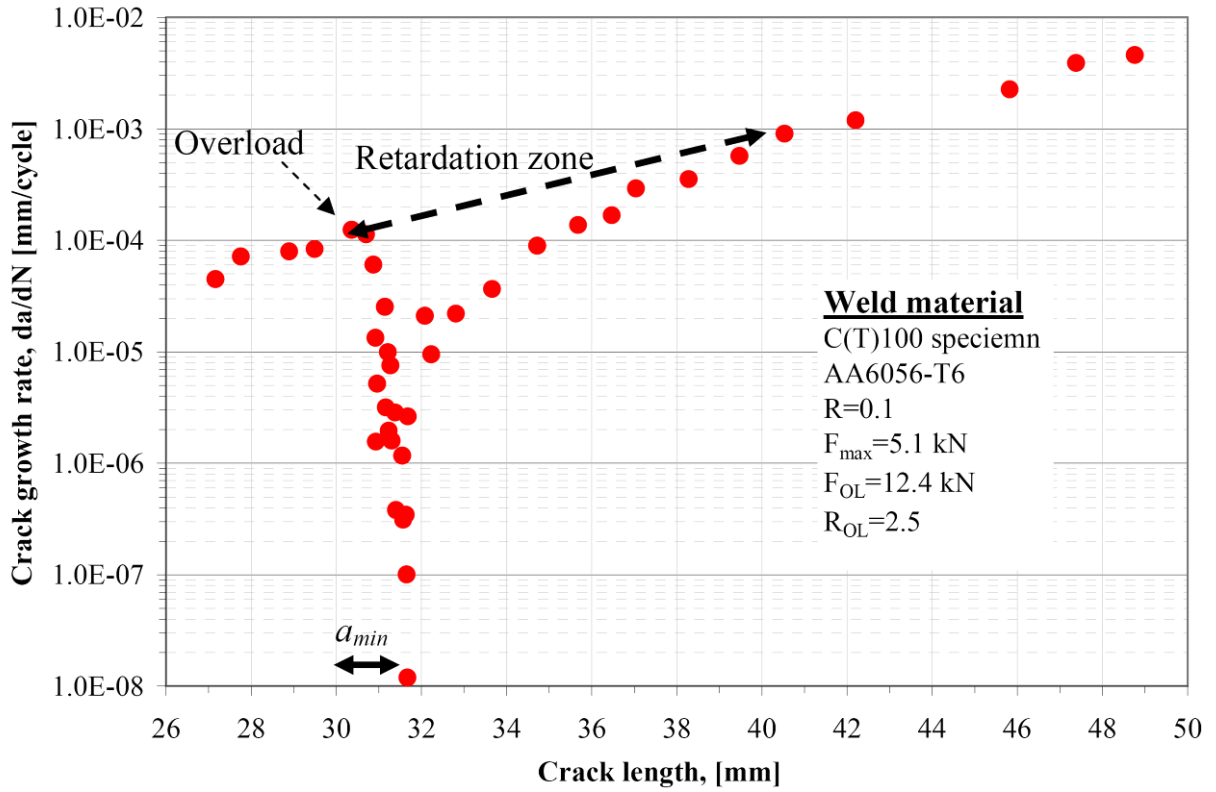Fig. 7. Crack growth rate versus crack length for base material, R_{OL}=2.5

Fig. 8. Crack growth rate versus crack length for weld material, R_{OL}=2.5

The retardation effect due to overload is evident in both base and weld material, where the minimum crack growth rate is reached at a certain distance known as "delay distance" [20] from the overload location ($a_{overload}$=30). After that, the crack growth rate recovers rapidly and then gradually approaches the well-known crack growth behavior at constant amplitude loading. A comparison of the observed behavior presented in Figs. 7 and 8 reveals four major differences between the crack growth rate in weld and base material in terms of (i) delay distance, (ii) magnitude of minimum growth rate occurred after overload, (iii) size of retardation zone, and (iv) slope of recovery of growth rate. The size of the retardation zone (see Fig. 7 and 8) in the welded specimen is larger than that in the base material and a longer delay distance at lower magnitude of minimum growth rate is observed in weld material.

According to these observations, a typical retardation zone as shown in the Fig. 1b can be assumed for both base and weld material of AA6056-T6 subjected to the single tensile overload. There are three regions that can be distinguished on the curve:

- Region I: a short region observed immediately after application of overload with small amount of temporarily accelerated growth which primarily occurs during the application of the overload (from a_{OL} until point S in the Fig. 1b).

- Region II: a fast reduction in crack growth rate within a distance known as the delay distance to reach to the minimum growth rate (between point S and a_{min} in the Fig. 1b).

- Region III: restoration of growth rate from the minimum crack growth rate until the normal growth rate is reached (between a_{min} and point R in the Fig. 1b).

Material degradation in form of ductile damage is expected to occur during the application of overload within Region I. Its consequences on the formation of Region II are discussed in detail in the following.
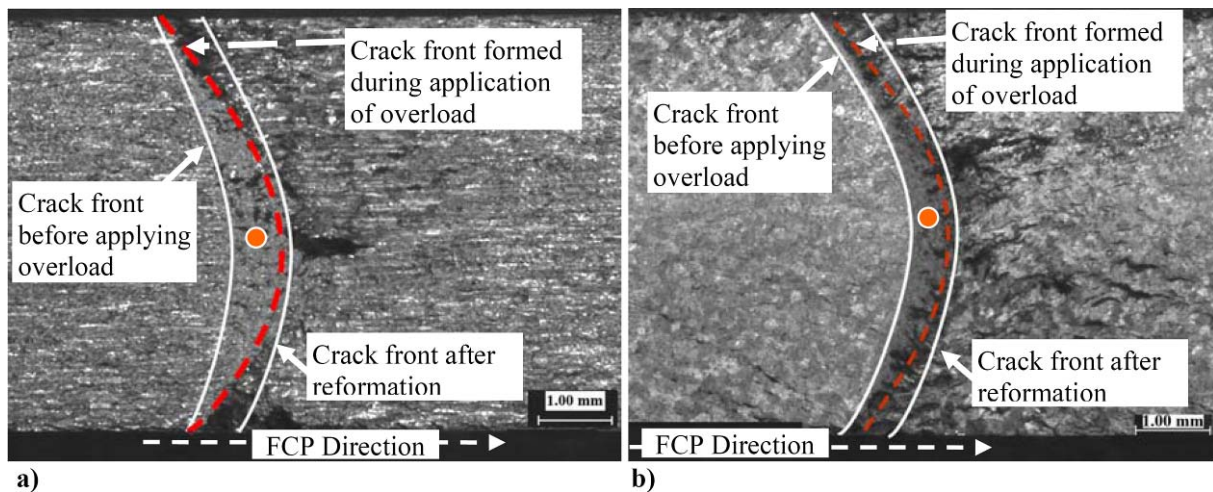
3.2. Fracture surfaces

An overview of the four fracture surfaces according to Table 1 is displayed in Fig. 9. The through thickness crack is initiated in the notched area in the left and grows in the right direction as shown in the Fig. 9. The location of the overload is visible as a dark, curved line. Comparing through thickness crack fronts for two different overload ratios reveals that in both types of specimen, the crack fronts are more curved for the higher overload ratio (see two left and two right fracture surfaces in the Fig. 9). This indicates the influence of overload magnitude on the shape of the crack front after application of the overload.
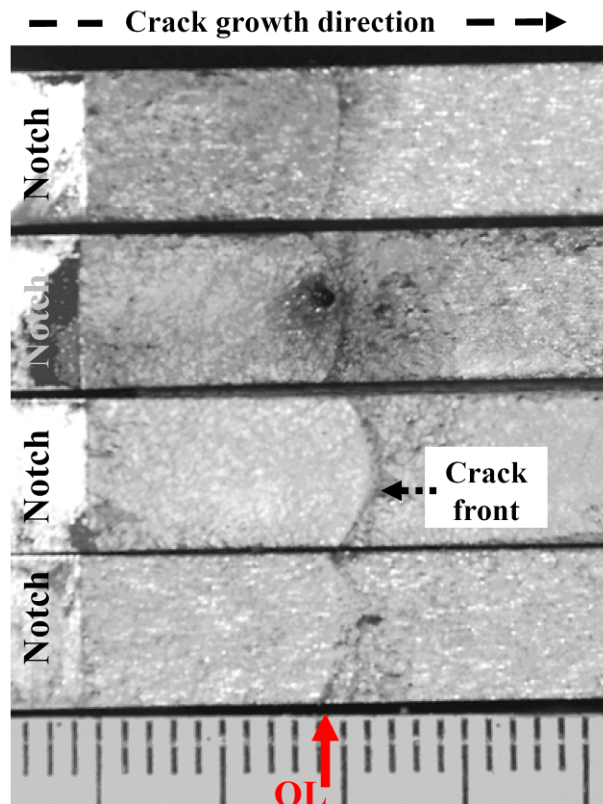
**Fig. 9. Fracture surfaces of C(T) 100 specimens of base material (BM) and weld material (WM) ;
From top: WM under $R_{OL}=2$, BM under $R_{OL}=2$, WM under $R_{OL}=2.5$ and BM under $R_{OL}=2.5$**

3.2.1 Reformation of crack front shape due to overload

Microscopy and SEM of the fracture surfaces reveal some notable features. One important effect is the shape change of the crack front before, during and after the overload. Fig. 10 highlights the evolution of the curvature of the crack front from the constant amplitude loading to single overload for both weld and base material. SEM images of the damage zone, which has formed during the application of the overload, are shown in Fig. 11. The boundary of this so-called overload zone is marked in the Fig. 10 by a dashed line. According to the Fig. 11, the overload zone in the base material (Fig. 11a) contains a dimple structure originated from secondary phase-particles. The overload zone in the weld material (Fig. 11b) consists of mainly fine dimple structures. During the welding of AA6056–T6 Al alloys, the precipitated secondary phase-particles, which are responsible for hardening, are dissolved in the matrix. No particles are left for generation of dimples. As a consequence a finer dimple structure without particles is observed in the case of the weld material, Fig. 11b. The existence of dimples in the overload zone of the fracture surface indicates a ductile damage as it is known from the fracture surface of a tensile test.


Fig. 10. Crack front shape in a) base material b) weld material; Marker indicates position in the overload zone, which is shown in a higher magnification in Fig. 11

a)   b)
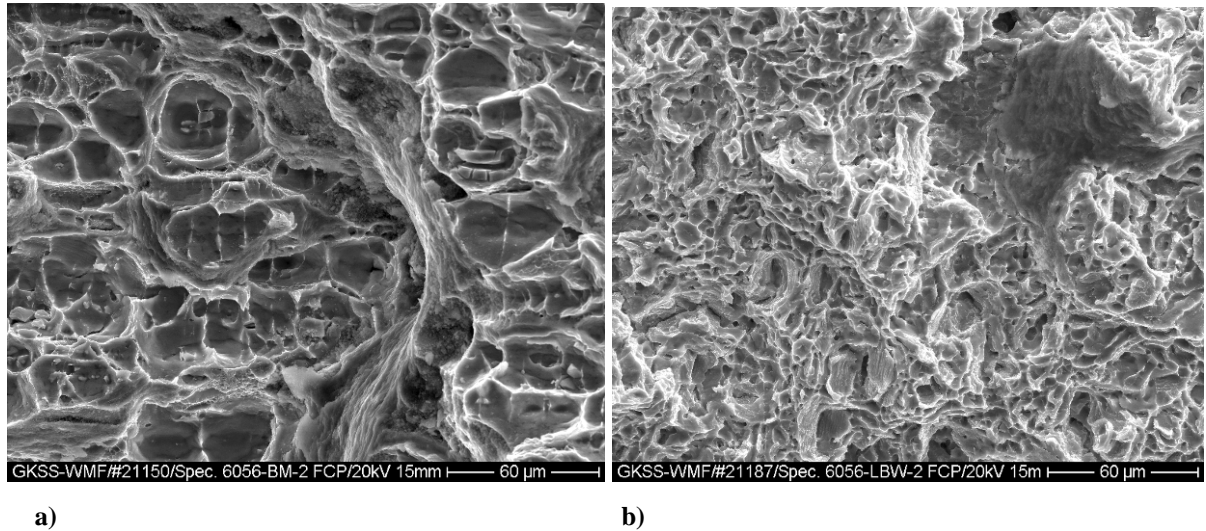
Fig. 11. Fracture surface of overload zone, marked in the Fig. 10, in a) base material b) weld material; The overload zone contains a dimple structure with a type of ductile failure typically observed in monotonic tensile loading.

A FE simulation based on the GTN model explained in the section 2.2 was performed to determine quantitatively the deformation and damage fields resulting from the overload. Figure 12 shows the damage distribution predicted for the base material after the application of the single overload. According to Fig. 12, the damage profile that has been observed in the experiment is in good agreement with the FE results. It is even possible to identify further features in the fracture surface, which are beyond the black curve and which were not clearly visible with out a guiding plot from the simulation.
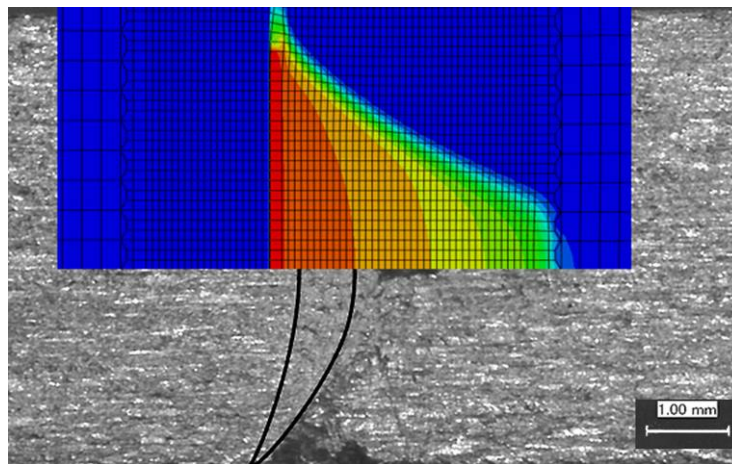
Fig. 12. Damage profiles formed during the application of the overload in base material; simulation against experiment.

The reason of having a curved crack front can be explained by the well-known change in the magnitude of stress triaxiality at the crack tip throughout the thickness of the specimen: plain stress at the specimen surface against plain strain in the centre of the specimen. For a

13

specimen of a given thickness, the shape of the crack front depends on the level of applied load and, as a consequence, is of increasing curvature with increasing load.

What is now observed during the single overload is a jump forward so the curve of the crack front changes within one half cycle. The resulting crack front, which incorporates the newly formed damage zone, is more curved than the initial crack front. Once the specimen is again subjected to constant amplitude cyclic loading with a lower load amplitude, the shape of the crack front slowly returns to its initial shape. During this reformation process of the cack front, a non-uniform through thickness crack growth is supposed to take place directly after applying overload. The reformation of the initial crack front shape dissipates a portion of the energy and leads to a delay in crack growth after the applied overload. The zone formed during the reformation process is called transition zone.

3.2.2 Delay in transition zone

The area, which is trapped between the monotonic crack fronts formed during the application of the overload and the one formed after reaching again the stable crack front shape under constant amplitude loading is called transition zone. SEM images of the fracture surface indicate the transition zone as darker regions in the outer layers of the specimen in both weld and base material as shown in Figs. 13a and 13c. The fracture surfaces of the transition zone in both weld and base material shown in Figs. 13b and 13d are smooth and flat. It is likely that the crack flanks within this zone come locally into contact (local crack closure). The striated fracture surface in the weld material (Fig. 13d) appears much more flat and darker and seems to be severely damaged. Based on the SEM observations, the failure within the transition zone is characterized by a severely damaged and subsequently flattened surface with local contacts of crack flanks.
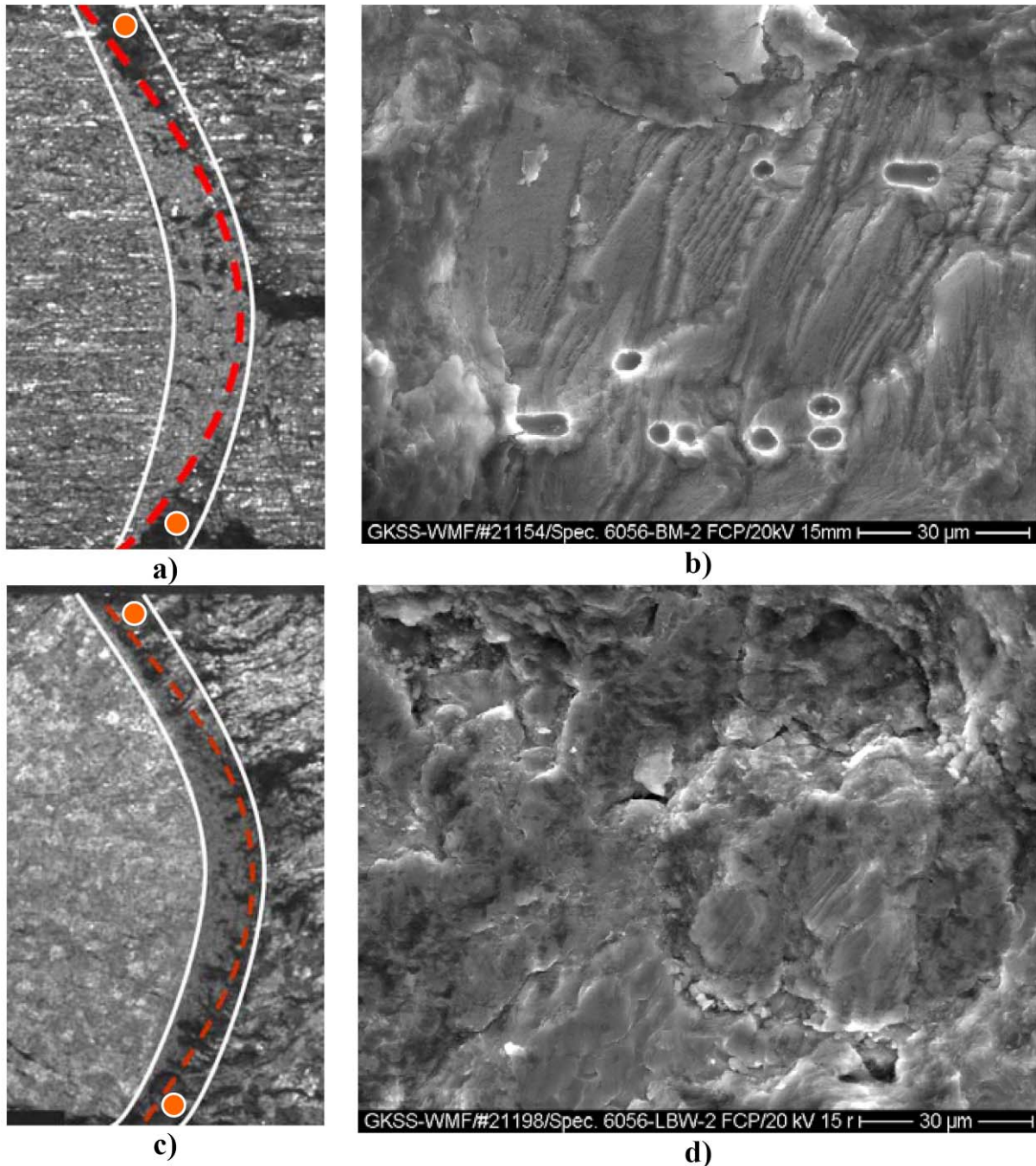
Fig. 13. a and c) Overviews of fracture surfaces in base and weld material respectively; Fatigue damage observed by SEM within transition zone, marked by ⬤ in b) base material and d) weld material.

Figure 14 shows the correlation between the crack growth rate and the correlation with the fracture surface of the C(T) 100 specimen for the base material. It can be seen that the transition zone almost perfectly aligns with the deceleration region (region S-M in Fig. 1b) of the plot that is showing a similar size of delay distance and transition zone.

Delay in crack growth observed within transition zone can be attributed to the time which is needed for reforming the crack front after the application of the overload. During this time the crack front at the centre of the specimen remains almost immobile.

The inhomogeneous plastic deformation, which has been generated in front of the crack tip during the application of the overload, introduces also compressive residual stresses in a larger volume around the crack tip. These compressive residual stresses reduce the local crack tip loading and retard the crack growth in its restored shape during the following fatigue loading.
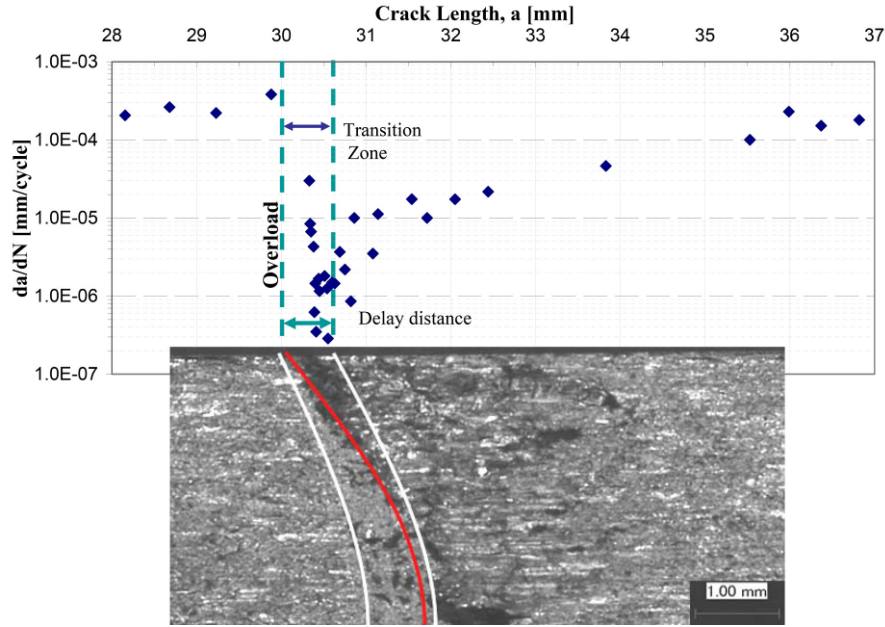
Fig. 14. Correlation between crack growth rate and fracture surface in AA6056-T6; within the transition zone; the delay in this zone is closely related to the reformation of the crack front.

4. Conclusions and outlook

In this study investigations were carried out on the crack retardation phenomenon due to tensile overload in base material and laser welded AA6056-T6. The amount of crack retardation was compared for two different overload ratios. A FE analysis was performed to determine the plastic deformation and resulting damage profile caused by an overload. The following conclusions can be drawn from this study:

- Tensile overload causes more significant crack retardation in the undermatched laser welds of AA6056-T6 than in base material. The application of a tensile overload induces a large crack tip plasticity confined to the weld zone which is elongated ahead of the crack tip, resulting in significant crack retardation and longer fatigue life in the laser welded specimens.
- Tensile overload changes the shape of crack front and form a more curved crack front due to ductile damage.

16

- During the application of overload in both weld and base material, a damage zone called overload zone is formed ahead of the crack tip. The fracture surface of this zone is characterized by dimple structure which is very similar with the fracture surface induced under monotonic tensile loading.

- The GTN damage model based on the porous metal plasticity can be used to predict the damage profile and the shape of crack front formed during the application of overload.

- The process of reformation of the crack front after overload leads to a visible retardation of post overload crack within the time until reaching to the minimum crack growth rate.

- A correlation has been observed between the crack growth rate and the fracture surface of overloaded specimen. A similar size of delay distance and transition zone is observed.

A quantitative prediction of fatigue crack propagation through the damaged and plastically deformed zone based on the presented FE model is planned for future work. It is expected by such an approach to consider the influence of damage, compressive residual stress, crack closure, crack tip blunting, and work hardening of material ahead of the crack tip. The goal of this work will be a quantitative prediction of crack retardation and delay simultaneously with the simulation of crack growth.

5. Acknowledgments

6. References

[1] S. Daneshpour, M. Koçak, S. Langlade, M. Horstmann, Effect of overload on fatigue crack retardation of aerospace Al-alloy laser welds using crack-tip plasticity analysis, Int. J. of Fatigue 31 (2009) 1603–1612.

[2] J.A. Bannantine, J.J. Comer, J.L. Handrock, Fundamentals of metal fatigue analysis, prentice-Hall Inc., USA, 1990.

[3] R. Kocik, T. Vugrin, T. Seefeld, Laserstrahlschweißen im Flugzeugbau: Stand und künftige Anwendungen, 5. Laser-Anwenderforum, Bremen-Germany, 13-14.09.2006.

[4] G. Tempus, New Aluminum Alloys And Fuselage Structures In Aircraft Design, Werkstoffe Für Transport Und Verkehr, ETH Zürich, Switzerland, 18.05.2001.

[5] M.V. Uz, M. Koçak, F. Lemaitre, J.C. Ehrstöm, S. Kempa, F. Bron, Improvement of Damage Tolerance of Laser Beam Welded Stiffened Panels for Airframes via Local Engineering, Int. J. of Fatigue 31 (2009) 916-926.

[6] T. Lassen, N. Recho, Fatigue life analyses of welded structures, ISTE Ltd, UK, 2006.

[7] W. Elber, Fatigue crack closure under cyclic tension, Eng. Fract. Mech. 2 (1970) 37–45.

[8] S. Matsuoka, K. Tanaka, M. Kawahara, The retardation phenomenon of fatigue crack growth in HT80 steel, Eng. Fract. Mech. 8 (1976) 507–23.

[9] O.E. Wheeler Spectrum loading and crack growth, J. Basic Eng. Trans. ASME 1(1972) 181–6.

[10] J. Willenborg, R.M. Engle, K.W. Liu, A crack growth retardation model using an effective stress concept, AFFDL TM-71-1-FBR, 1971.

[11] B.C. Sheu, P.S. Song, S. Hwang, Shaping exponent in Wheeler model under a single overload, Eng. Fract. Mech. 51 (1995) 135–43.

[12] Y. Lu, K. Li, A new model for fatigue crack growth after a single overload, Eng. Fract. Mech. 46 (1993) 849–856.

[13] R.G. Christensen, Fatigue crack, fatigue damage and their detection, Metal Fatigue, New York: McGraw-Hill, 1959.

[14] J.F. Knott, A.C. Pickard, Effect of overloads on fatigue crack propagation -aluminum alloys, Metal Science 11 (1977) 399-404.

[15] W. Elber, The significance of fatigue crack closure, ASTM STP 486 (1971) 230-42.

[16] W. Sun, H. Sehitoglu, Residual stress fields during fatigue crack grow, Fatigue Fract. Engng. Mater. Struct. 15(1992) 115-28.

[17] P. Staron, W.V. Vaidya, M. Koçak, Precipitates in laser beam welded aluminium alloy AA6056 butt joints studied by small-angle neutron scattering, Materials Science and Engineering A 525 (2009) 192–199.

[18] Standard test method for measurement of fatigue crack growth rates, ASTM E647-00, West Conshohocken (PA): American Society for Testing & Materials, 2000.

[19] A.L. Gurson, Continuum Theory of Ductile Rupture by Void Nucleation and Growth: Part I—Yield Criteria and Flow Rules for Porous Ductile Materials, J. of Enging. Materials and Technology 99 (1977) 2–15.

[20] S. Suresh, Fatigue of materials, Cambridge University Press, 1991.